journal

J. Am. Ceram. Soc., 89 [9] 2787–2795 (2006)
DOI: 10.1111/j.1551-2916.2006.01185.x

Modeling Electrophoretic Deposition on Porous Non-Conducting Substrates Using Statistical Design of Experiments

Charles Compson and Meilin Liu†

School of Materials Science & Engineering, Georgia Institute of Technology, Atlanta, Georgia 30332-0245

Laxmidhar Besra

Regional Research Laboratory (CSIR), Bhubaneswar 751013, India

David Earl

School of Engineering, Alfred University, Alfred, New York 14802

Statistical design of experiments was used to model electrophoretic deposition of yittria-stabilized zirconia (YSZ) particles on porous, non-conducting NiO–YSZ substrates. A 2^3–full-factorial matrix with three repetitions of the centerpoint was augmented with six axial runs and two additional centerpoints to form an inscribed central composite design. Fixed ranges of substrate firing temperature (1100°–1300°C), deposition voltage (50–300 V), and deposition time (1–5 min) were used as the independent design variables to model responses of YSZ deposition thickness, area-specific interfacial resistance (ASR), and power density. Regression equations were determined, which were used to optimize deposition parameters based on the desired responses of low interfacial polarization resistance and high-power density. Low substrate firing temperature (1100°C) combined with a low voltage (50 V) and minimal deposition time (1 min) resulted in a 6 μm-thick YSZ film, a power density of 628 mW/cm^2, and an ASR of 0.21 Ω·cm^2. Increasing the substrate firing temperature, voltage, and time to 1174°C, 215 V, and 3 minutes, respectively, reduced the ASR to 0.19 Ω·cm^2, increased YSZ film thickness to 25 μm, but had only a negligible effect on power density (600 mW/cm^2).

I. Introduction

SOLID OXIDE FUEL CELLS (SOFCs) have great potential to be an alternative power-generation source.[1,2] These fuel cells operate at high temperatures and offer greater fuel versatility and higher power density than other fuel cell technologies. Despite their several advantages, high fabrication costs[3,4] are still an obstacle that has to be overcome before SOFCs are cost competitive with current technologies. In recent years, traditional ceramic processing techniques have become popular methods for fabrication of planar SOFCs.[5–7] Techniques such as tape-casting, screen-printing, and electrophoretic deposition (EPD) have all been explored, due to their successes in lowering fabrication costs in other industries. Combinations of these traditional techniques, along with co-firing, may lead to reduced SOFC fabrication costs.[8]

Much work has been conducted on fabrication of SOFCs by EPD. Initially, only cathode-supported SOFCs could be fabricated due to the fundamental requirement of a conductive substrate for deposition. Ishihara *et al.*[9–11] and Chen *et al.*[12] determined that the EPD technique was capable of fabricating high-power density SOFCs, when they deposited a yittria-stabilized zirconia (YSZ) film of less than 10 μm on $La_{1-x}Sr_xMnO_3$ cathode substrates. Despite their high-power density, cathode-supported SOFCs lack the mechanical integrity of anode and electrolyte-supported cells. Zhitomirsky and Petric[13] therefore investigated the deposition of different fuel cell materials on conductive Ni–YSZ anode substrates. Will *et al.*[14] pre-sintered NiO-YSZ anode substrates at varying temperatures to create porosity and then reduced them in hydrogen before deposition of YSZ. Kobayashi *et al.*[15] and Yamaji *et al.*[16] performed similar depositions, substituting scandia-stabilized zirconia (SSZ) for YSZ due to its higher ionic conductivity. This was taken a step further by Matsuda *et al.*[17], who performed depositions of YSZ on porous NiO-YSZ substrates after applying a thin coating of carbon on the reverse side. Our experimental setup is similar to those of Will,[14] except that the anode substrates were non-conductive, and Matsuda,[17] except that a conductive layer was not applied to the back of the substrate.

Statistical design of experiments can be used for optimization of linear and non-linear systems.[18] Factorial designs allow the effects of several different factors to be analyzed and combined into a response model. To create a 2^k factorial design, all combinations of k-factors set at two different levels with respect to a central point are evaluated and the response must be assumed to be relatively linear over the range of factor levels. Although typically used for screening experiments rather than surface response modeling, 2^k factorial designs are easily augmented and/or modified to form robust designs.[18] Augmentation with centerpoint replicates allows for an estimate of pure experimental error and detection of curvature from second-order effects. Improved models for non-linear effects are achieved through augmentation into central composite designs (CCDs).[19]

In this report, we discuss recent work involving statistical experimental design and modeling of YSZ deposition on porous non-conducting substrates. Preliminary results were reported earlier;[20] however, the significant experimental factors and effects leading to YSZ deposition were not determined. A comprehensive analysis of the data has resulted in a series of regression models, which can be used to improve the deposition process and better achieve the desired response.

II. Experimental Procedure

A 2^3 factorial design with the addition of three centerpoint experiments was used to determine both main and interaction effects on particle deposition. Design Expert v.7 statistical software (Stat-Ease Inc., Minneapolis, MN) was used to determine the geometric notation and coded notation as well as randomize

R. Cutler—contributing editor

Manuscript No. 21365. Received January 10, 2006; approved May 22, 2006.
†Author to whom correspondence should be addressed. e-mail: meilin.Liu@mse.gatech.edu

the treatment combinations, resulting in a standard and experimental order. After all the experiments were conducted, the desired responses of power density, area-specific interfacial resistance (ASR), and deposition layer thickness were input into the factorial matrix, diagnosed and modeled using the software. Factor effects with a significance level of 0.05 or lower (p-value ≤ 0.05; 95% confidence level) were included in the regression models.

Porous NiO-YSZ substrates were formed via tape casting. Commercial NiO powder (97%, Alfa Aesar, Ward Hill, MA) with a particle size of less than 10 μm was too large for stable dispersion within a slurry and therefore was ball-milled in ethanol, using 6 mm YSZ charge, for 96 h. The milled NiO powder was then dried, ground in a mortar and pestle, and mixed with YSZ powder. The YSZ powder (8 mol%, Daiichi Corporation, Tokyo, Japan) with a median particle size of 0.26 μm was dried for 48 h at 120°C before use ensuring removal of any surface hydroxyl groups. NiO and YSZ powders were mixed in a stoichiometric ratio that would produce a 1:1 volume ratio of Ni to YSZ after reduction. EPD was performed using a 10 g/L suspension concentration of YSZ in acetylacetone under constant stirring and at an electrode spacing of 1 cm. The suspension was ultrasonicated for 20 min before deposition, 5 min between depositions, and replenished after every five deposits.[20] The samples were then co-fired at 1400°C for 5 h before $La_{0.85}Sr_{0.15}MnO_3$:YSZ composite cathodes (1:1 ratio) were brush painted on the electrolyte. The composite cathodes were sintered at 1250°C for 2 h and then the cell was sealed to an alumina tube using a silver paste (C8710, Heraeus Cermalloy, W. Conshohocken, PA) as described elsewhere.[20]

Before fabricating the treatment combinations, some brief screening experiments were conducted to determine reasonable factor levels and the centerpoint placement. Depositions of YSZ were performed on porous NiO–YSZ pellets using varying voltages (25–500 V) and times (30 s to 5 min). The resulting green deposit was observed for substrate coverage, consistency, and uniformity.[20] After the preliminary depositions were completed, high and low levels were chosen for each factor. The levels for factor A (substrate firing temperature) were chosen based on characterization of the substrate porosity and ranged from 1100° to 1300°C. Factor B (deposition voltage) and Factor C (deposition time) were chosen to range between 50–300 V and 1–5 min, respectively. SOFC performance and impedance spectroscopy characterization were measured using a Solartron 1287 electrochemical interface (Solarton Analytical, Farnborough, Hampshire, U.K.) and Solartron 1255 frequency response analyzer running Corrware and Zplot software, respectively. The characterization range was from 550° to 850°C, with humidified hydrogen (3 vol% H_2O) as the fuel and air as the oxidant. Although the samples were characterized over a range of temperatures, statistical models were only prepared for the highest operating temperature, in this case 850°C.

III. Statistical Design and Modeling

(1) Full Factorial Design

A 2^3 factorial design was chosen to model particle deposition because it provided the minimum number of experiments for which linear effects and interactions of all factors could be investigated. Each factor was run at two levels and the intermediate response was assumed to be linear, which is necessary for 2^k designs. The assumption of linearity is considered valid for such responses as open-circuit voltage and substrate density, but may not be valid for deposition thickness and power density. There are methods to account for potential non-linearity within the design space, mainly through the introduction of centerpoints and model augmentation. Centerpoints are essentially used to test for evidence of pure second-order or quadratic effects in the response region of exploration, represented by the regression coefficient β_{jj}. Therefore, three repetitions of the centerpoint were added to the 2^3 factorial design. Centerpoint placement within the experimental order can be random or non-random depending on a number of considerations. Randomizing the centerpoint runs allows the determination of linearity within the design matrix. Addition of centerpoints to the design matrix allows for determination of unusual occurrences throughout the experiments. In a well-known process, the centerpoint is often the normal operating condition, and periodic placement (non-randomly) ensures negligible deviation from operating standards.[18] Plotting the periodic centerpoint responses in order can reveal abnormal baseline trends and experimental stability. When a new process is being used, the centerpoint experiments can be front loaded in the run order to determine the magnitude and reasonableness of the variability. As the EPD process was well known, but deposition on non-conducting substrates was unknown, two centerpoint experiments were conducted at the beginning of the run order while a third was inserted randomly.

After completion of all factorial experiments and centerpoint runs, the treatment responses were used to determine the degree of main and interaction effects within a regression model. Analysis of variance was completed and models were generated for the responses of deposition thickness, power density, and interfacial resistance, with each model indicating that all factors and interactions were significant. Table I shows the initial analysis of variance results for deposition thickness. The regression model was only significant if all of the linear, interaction, and curvature terms were simultaneously included. However, there were insufficient degrees of freedom remaining to calculate the mean square error, which is the value representing the total model error. With a model error value of zero, unrealistically large F values and R^2 and adjusted R^2 values of unity resulted. F values are calculated by dividing the mean square value for a factor by the mean square error for the entire model; therefore, the F values would be driven to infinity with a mean square error of zero. The maximum F values that could be output by the statistics

Table I. Analysis of Variance of 2^3 Full Factorial Model

Source	Sum of squares	Degrees of freedom	Mean square	F-value	p-value Probability $>F$
Model	1541.671	7	220.239	63 660 000	<0.0001
Firing temperature	787.847	1	787.847	63 660 000	<0.0001
Voltage	317.394	1	317.394	63 660 000	<0.0001
Time	16.217	1	16.217	63 660 000	<0.0001
Firing temperature × voltage	165.529	1	165.529	63 660 000	<0.0001
Firing temperature × time	37.802	1	37.802	63 660 000	<0.0001
Voltage × time	158.509	1	158.509	63 660 000	<0.0001
Firing temperature × voltage × time	58.374	1	58.374	63 660 000	<0.0001
Curvature	13.924	1	13.924	63 660 000	<0.0001
Pure error	0	2	0		
Cor total	1555.595	10			

Note that the F-values listed are at the largest value allowed by the software and were driven to infinity as a result of insufficient degrees of freedom necessary to calculate the mean square error.

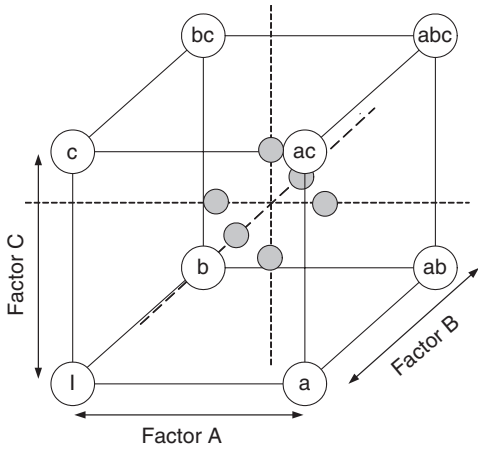

Fig. 1. Inscribed central composite design matrix resulting from augmentation of the 2^3 factorial design.

software are displayed. Required mutual inclusion between the factors and interactions indicates that not enough information was present to form an accurate response model. Similar results were obtained for the analysis of variance of the power density and ASR responses.

(2) Design Augmentation

The factorial model was therefore augmented with six axial runs and two additional centerpoints, forming a CCD. In addition, the original 2^k factorial experiments were repeated in order to validate the initial findings and potentially reduce model prediction error. The choice of CCD (spherical or cuboidal) depends mainly on whether the resulting design matrix needs to be rotatable and whether the design region encompasses non-allowable conditions. Rotatable designs have equivalent prediction error for all design points, which is desired for optimization within an unknown system, and yet necessitates more design runs and may not result in a significant reduction in prediction error compared with cuboidal or non-rotatable CCDs.[18,19,21] As two faces of the factorial matrix were near the extremes of allowable operation, an inscribed CCD was chosen. Inscribed CCDs are rotatable and allow the experimenter to utilize data points at or near non-allowable operating conditions. Six inscribed design points were added randomly at coded factor levels of $\alpha = \pm 0.7$, along with two additional centerpoints. The inscribed CCD matrix and augmented treatment combinations are shown in Fig. 1 and Table II, respectively.

IV. Design Models

(1) Deposit Thickness

Deposit thickness has a linear relation with deposition time[14] and the amount of charge passed.[14,22,23] The statistical analysis in the present study also identified significant two-factor interactions. Figures 2(a)–(c) shows the surface response and interaction plots for the regression model for deposition thickness. Interaction plots were generated from model predictions by holding the factor not included in the plot at its intermediate level. Based on trends observed in the diagnostic residual and Box–Cox plots, no transform of the raw data was necessary. The diagnostic plots therefore had a normal distribution, with the exception of experimental run #3, which will be discussed later. The regression equation for deposition thickness is

Table II. Augmented Design in Actual Terms

Standard order	Experiment order	Substrate firing temperature (°C)	Deposition voltage (V)	Deposition time (min)	Power density (mW/cm^2)	Area-specific resistance ($\Omega \cdot$ cm^2)	Deposition thickness (μm)
9	1	1200	175	3	447	0.19	20
10	2	1200	175	3	442	0.191	20.2
8	3	1300	300	5	10	6.7	6.3
7	4	1100	300	5	406	0.47	38
3	5	1100	300	1	45.5	0.46	40.5
1	6	1100	50	1	611	0.215	5.3
5	7	1100	50	5	232	0.75	25
11	8	1200	175	3	442	0.191	20.2
2	9	1300	50	1	6.2	5.4	24
4	10	1300	300	1	0.7	5.9	11
6	11	1300	50	5	3	5.9	5.5
14	12	1100	50	5	224	0.72	27.5
18	13	1300	300	1	3.1	7.1	12
15	14	1300	300	5	5.2	6.1	7
19	15	1300	50	5	7	4.3	7
12	16	1100	50	1	628	0.21	6
17	17	1200	175	3	452	0.187	19.6
13	18	1100	300	5	404.7	0.44	38
16	19	1100	300	1	38	0.46	42
23	20	1200	262.5	3	35	2.9	23
26	21	1200	175	3	449	0.192	19.9
27	22	1200	175	3	431	0.189	20
24	23	1200	175	1.6	210	0.32	19
22	24	1200	87.5	3	100	1.2	14.6
25	25	1200	175	4.4	160	0.86	21
21	26	1270	175	3	80	2.7	13
20	27	1130	175	3	450	0.3	26
28[†]	28[†]	1174	216	3	616	0.192	26

[†]Model validation experiment.

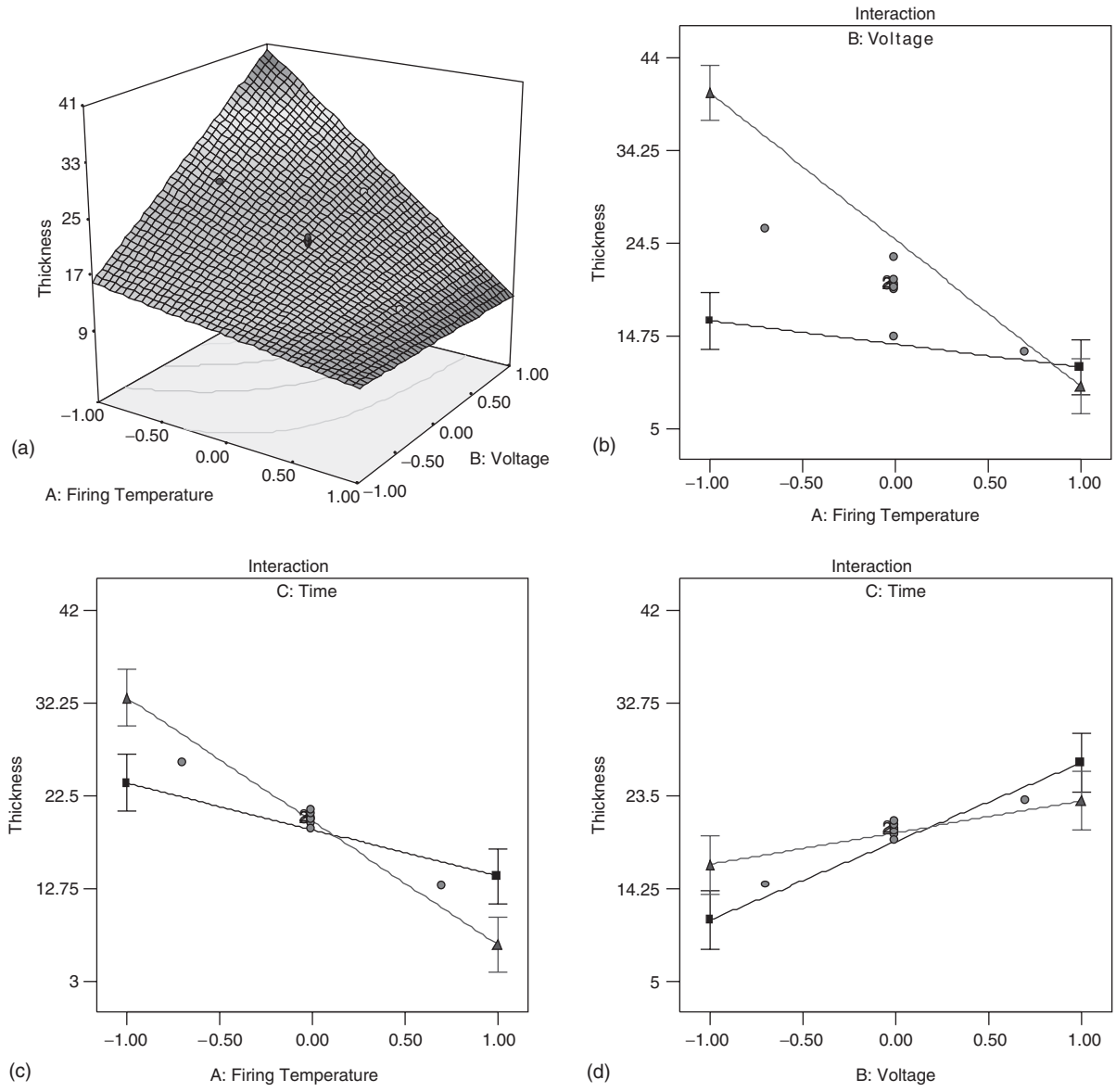

Fig. 2. (a) Surface response plot for deposit thickness model along with the (b) single factor and (c,d) interaction plots. Note that for single factor and interaction plots, ▲ represents the high factor level and ■ represents the low factor level.

$$\begin{aligned}\text{Thickness} = & 19.40 - 8.87(\text{firing temperature}) \\ & + 5.45(\text{deposition voltage}) + 0.41(\text{time}) \\ & - 6.5(\text{firing temperature} \times \text{deposition voltage}) \\ & - 4.06(\text{firing temperature} \times \text{deposition time}) \\ & - 2.3(\text{deposition voltage} \times \text{deposition time})\end{aligned}$$

As all of the linear effects and two-factor interactions were significant (the linear Time term remains in the model due to hierarchy) in the analysis of variance, as shown in Table III, the full and reduced models are identical. Quadratic terms were not significant and only increased the error if forced into the model. The fact that no quadratic terms were significant shows that the model follows a fairly linear trend between thickness and such variables as time and voltage, as mentioned previously. The linearity between thickness and time and indirectly between thickness and the amount of charge passed is demonstrated around the centerpoint, as shown in Figs. 3(a) and (b). The presence of interaction terms in the model gives rise to some curvature at the extreme factor levels, which is why a slight non-linearity is observed at the high and low levels of substrate firing temperature. The regression coefficients and their corresponding *t*-values are listed in Table IV. The reduced model statistics of standard error (4.32), R^2 (0.890), adjusted R^2 (0.855), and the signal-to-noise ratio (16.5) show that the model can account for nearly all the variability in the response data. The externally studentized residuals and Cook's distance plots did reveal one outlier point, experimental run #3 from Table II; however, the leverage plot did not indicate that the outlier influenced the response model more than any other data points. The outlier data point (experimental run #3) was replicated in experimental run #8, which resulted in a thickness value that appeared more suitable for the deposition parameters. Experimental run #8 is therefore considered a truer value for that treatment combination and we speculate that the high thickness value observed for the outlier run was the result of a greater than normal porosity in the substrate.

An increase in the substrate firing temperature inhibits deposition thickness as seen in the regression equation and Fig. 2(a). The reasoning for this is that as the substrate is fired at higher temperatures, the substrate porosity decreases. As the substrate firing temperature has such a large significance compared with the other factors listed in Table III, porosity is believed to be the

Table III. Analysis of Variance of Reduced Thickness Interaction Model

Source	Sum of squares	Degrees of freedom	Mean square	*F*-value	*p*-value probablity >*F*
Block	1.295	1	1.295		
Model	2868.757	6	478.126	25.58	<0.0001
Firing temperature	1337.485	1	1337.485	71.55	<0.0001
Voltage	503.684	1	503.684	26.94	<0.0001
Time	2.886	1	2.886	0.15	0.6988
Firing temperature × voltage	676.000	1	676.000	36.16	<0.0001
Firing temperature × time	264.063	1	264.063	14.13	0.0013
Voltage × time	84.640	1	84.640	4.53	0.0467
Residual	355.188	19	18.694		
Lack of Fit	212.087	8	26.511	2.04	0.1359
Pure error	143.102	11	13.009		
Cor total	3225.240	26			

most influential factor on YSZ deposition. The effect of porosity has not been completely quantified, however, because potential contributing effects of particle curvature can not be separated from the firing temperature factor. Although probably negligible compared with the porosity, the effects of firing temperature on particle curvature cannot be ignored.

Except at the highest firing temperature tested, voltage has a positive effect on deposition thickness, as increasing voltage will increase the particle transport[23,24] and deposition rates.[25] Reports have indicated that thickness varies linearly with voltage over a certain voltage range.[9,12] The surface response in Fig. 2(a) shows that the positive voltage effect lessens with increasing firing temperature and is negligible at the highest temperature. Conversely, the temperature effect is also reduced as the voltage is lowered. The changing effects correspond to the interaction term.

Deposition time has been reported previously to have a positive effect on thickness.[26] Most reports indicate that there is a linear relation between thickness and time under constant current and constant concentration conditions. The conditions used in these experiments were constant concentration, but not constant current and therefore a complete comparison could not be made. The relationship between the thickness and time appears to depend on the substrate firing temperature, as indicated by the significant interaction. For all substrates fired at the lowest level (1100°C), the deposition thickness varies linearly with deposition time. This is not the case, however, as the substrate firing temperature is increased. At higher levels of firing temperature the deposition thickness appears concave, leveling off just as seen in other reports.[17,26] Concavity within the deposition profile is probably due to the non-linear relation between the substrate firing temperature and the resulting substrate porosity.

All two-factor interactions were found to effect deposition thickness. The interactions of deposition voltage and time with firing temperature are significant because as the firing temperature increases, there is less porosity and therefore less ability for the conducting electrolyte to move through the substrate.[20] Subsequently, as firing temperature increases more voltage and time are necessary to build up a film deposit. Owing to the decrease in substrate porosity, however, the deposit thickness necessary to reduce the deposition rate is lessened. The deposition voltage–deposition time interaction results in a reduced layer thickness, which is not intuitive for the EPD process. The regression coefficient is the combination of the voltage–time interactions at each level of firing temperature. As the deposit thickness relates linearly with firing temperature only at the lowest level studied,

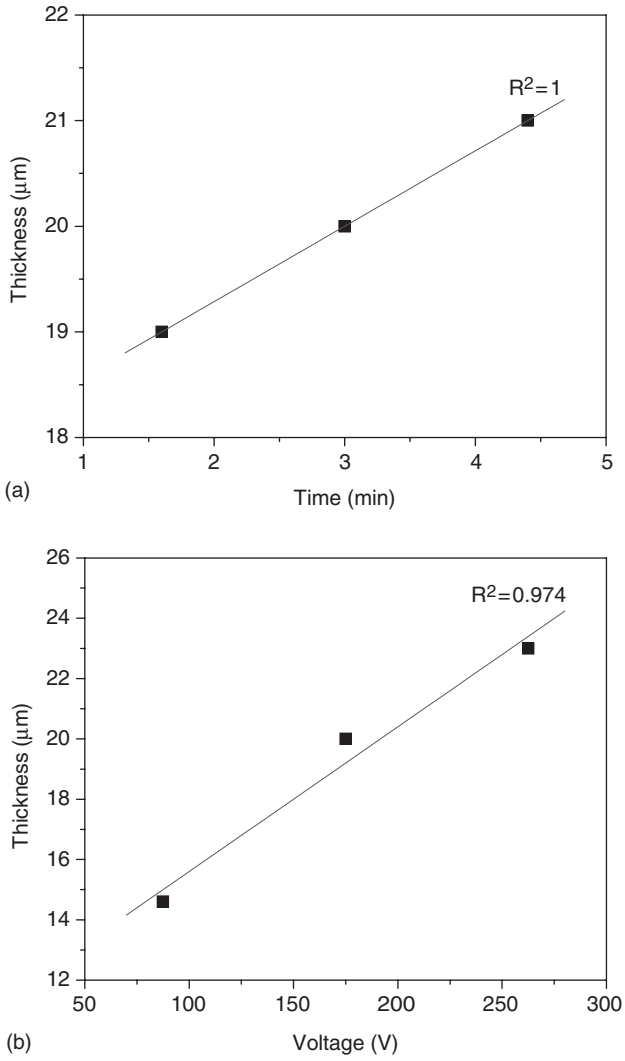

Fig. 3. Linear relationship between deposition thickness and (a) time and (b) voltage around the centerpoint experiments.

voltage and time effects only increase the thickness linearly at the lowest level of firing temperature. When the voltage–time interaction is studied at higher levels of firing temperature, the results are mixed. Lower values of the voltage–time interaction and higher levels of firing temperature typically lead to less particle velocity and deposition. The negative sign of this interaction coefficient therefore indicates the strong necessity of porosity for deposition, regardless of the voltage and time. High voltage and longer deposition time will still result in thin deposits even if the porosity is too low. This implies that there must be a critical porosity above which the voltage–time interaction has a positive effect and below which the voltage–time interaction has a negative effect. The response data indicate that the critical porosity level is achieved at temperatures near 1100°C.

Table IV. Thickness Model Regression Coefficients and Their Corresponding *t*-Values

Variable	Coefficient	*t*-value
Intercept	19.398	
Firing temperature	−8.875	−8.46
Voltage	5.446	5.19
Time	0.412	0.39
Firing temperature × voltage	−6.500	−6.01
Firing temperature × time	−4.063	−3.76
Voltage × time	−2.300	−2.13

Values of $|t| > 2.1$ indicate at least 95% confidence level. Regression model $R^2 = 0.890$, adjusted $R^2 = 0.855$. Standard error of model ($S_{y.x}$) = 4.324.

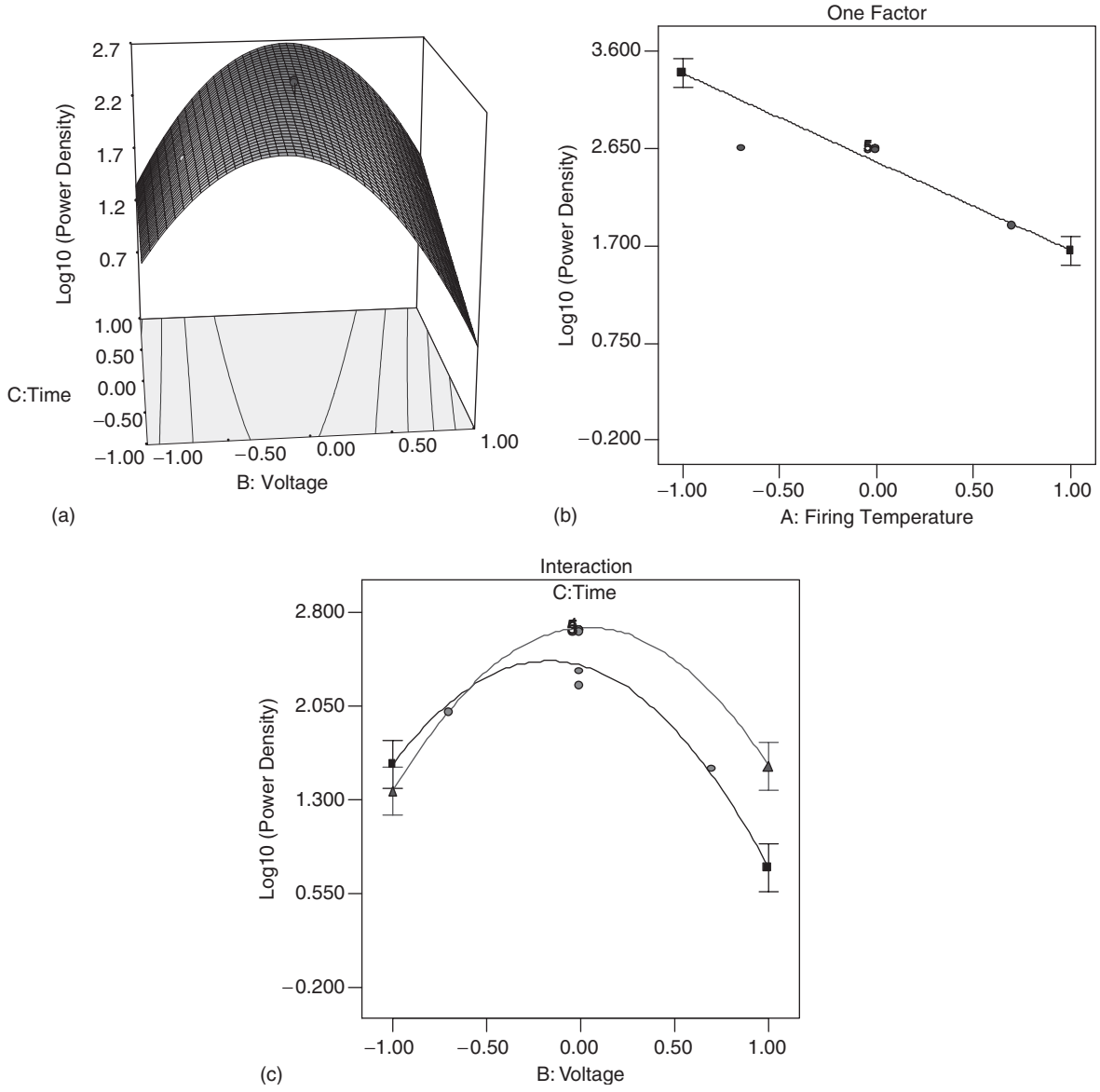

Fig. 4. (a) Surface response plot for power density model, along with the (b) single factor firing temperature and (c) deposition voltage–deposition time interaction plots. Note that for single factor and interaction plots, ▲ represents the high factor level and ■ represents the low factor level.

(2) Power Density

A regression model based on the main, interaction, and quadratic effects was developed from the observed power density responses. Analysis of variance of the full model revealed trends in the residual plots, suggesting that a variance-stabilizing transformation of the power density values should be performed before a regression model is developed. A Box–Cox plot indicated a logarithmic transform would be the most appropriate, which proved to negate any trends in the residual plots and normalize the data set. The regression equation in actual terms is given below and the surface response plot is shown in Figs. 4(a)–(c):

$$\begin{aligned}\text{Log}_{10}\,(\text{power density}) = {} & 2.52251 - 0.866518 \times \text{temperature} \\ & - 0.15462 \times \text{voltage} + 0.14949 \\ & \times \text{time} + 0.25586 \times \text{voltage} \\ & \times \text{time} - 1.20266 \times \text{voltage}^2\end{aligned}$$

Although the model contains a quadratic term and the R^2 values are very high, there is no evidence of "overfitting," which would be the case if the model error were significantly lower than the measured experimental error. The model error ($S_{y.x} = 0.232$) is not lower than the experimental error ($S_{test} = 0.190$) estimated by the pooled standard deviation of repeat experiments. The experimental error variance term (S^2_{test}) is also reported as the mean square pure error in the ANOVA, shown in Table V. The regression coefficients determined at a

Table V. Analysis of Variance of Reduced Power Density Quadratic Model

Source	Sum of squares	Degrees of freedom	Mean square	F_o-value	p-value probability $>F$
Block	1.983	1	1.983		
Model	18.757	5	3.751	69.70	<0.0001
Firing temperature	12.749	1	12.75	236.89	<0.0001
Voltage	0.406	1	0.406	7.54	0.0124
Time	0.379	1	0.379	7.05	0.0152
Voltage × time	1.047	1	1.047	19.46	0.0003
Voltage^2	4.175	1	4.175	77.57	<0.0001
Residual	1.076	20	0.054		
Lack of fit	0.678	9	0.075	2.08	0.1254
Pure error	0.398	11	0.036		
Cor total	21.816	26			

Table VI. Power Density Model Regression Coefficients and their Corresponding *t*-values

Variable	Coefficient	*t*-value
Intercept	2.523	
Firing temperature (°C)	−0.867	−15.39
Voltage (V)	−0.155	−2.75
Time (min)	0.149	2.66
Voltage × time (V · min)	0.256	4.41
Voltage^2 (V^2)	−1.203	−8.81

Values of $|t| > 2.1$ indicate at least 95% confidence level. Regression model $R^2 = 0.946$, adjusted $R^2 = 0.932$. Standard error of model ($S_{y.x}$) = 0.232.

95% confidence interval and their corresponding *t*-values are listed in Table VI.

Model reduction led to little change in the amount of variability explained by the model. Reducing the model slightly decreased the R^2 statistic from 0.953 to 0.946, but the standard error was favorably lowered from 0.242 to 0.232. The adjusted R^2 statistic was 0.932 after reduction, correlating very well with the reduced model R^2 statistic. Other model statistics such as the predicted error sum of squares (PRESS) and predicted R^2, and their correlation with the R^2 and adjusted R^2 statistics, indicated that the reduced model is a good predictor and that reduction increased the model's ability to explain variability in new data. Diagnostic plots of the reduced model with a logarithmic transform of the density values showed an as-expected normal probability plot of residuals as well as structureless residual plots. Although two data points appeared separate from the other responses in the leverage plots, they were not outliers and the overall model lack of fit is insignificant.

As seen in the regression equation for the reduced model, all main effects as well as the voltage–time interaction and the voltage quadratic term were significant. Insignificant factors were the substrate firing temperature interaction effects and the quadratic factors for the substrate firing temperature and deposition time. Overall, the power density increases as the substrate firing temperature is decreased. A decrease in the firing temperature leads to increased porosity and therefore increased mobility of the conducting species within the substrate, which results in a more uniform and densely packed deposit. This correlates well with our proposed deposition mechanism on porous non-conducting substrates,[20] which states that adequate porosity will allow deposition to occur even in the absence of substrate conductivity. The highest and lowest power densities were observed at the lowest and highest levels of substrate firing temperature, respectively, which explains why it has the largest *t*-value of all significant effects. Further decreases in substrate firing temperatures could potentially increase power density; however, experimentally, these samples were not mechanically able to withstand the spring forces in the EPD apparatus and also lacked the microstructural phase connectivity necessary for percolation in the anode.[20]

Table VIII. Area-Specific Resistance Model Regression Coefficients and their Corresponding *t*-Values

Variable	Coefficient	*t*-value
Intercept	0.474	
Firing temperature	2.653	19.76
Voltage	0.331	2.47
Firing temperature × voltage	0.285	2.06
Voltage^2	2.943	9.04

Values of $|t| > 2.1$ indicate at least 95% confidence level. Regression model $R^2 = 0.958$, adjusted $R^2 = 0.950$. Standard error of model ($S_{y.x}$) = 0.553.

Deposition voltage has a non-linear effect on power density, with a strong voltage–time interaction. Although the single highest power density observed during the experiments was at the lowest voltage, model predictions shown in Fig. 4(a) indicate that the lowest voltage level may not be optimal. Voltage only relates to the deposit through its influence on the electric field. As the electrode spacing remained constant throughout all experiments, the effect of the electric field is proportional to the applied voltage. The voltage and, further, the electric field present in the suspension, effectively influence the mobility of the particles and how fast they deposit. Higher deposition voltages lead to higher mobilities but do not necessarily allow the particles time to pack together.[23,26,27–30] Typically, lower voltages lead to increased deposit density due to increased particle packing.[9–11,13–17,20] Deposition time itself will lead to a sufficiently thick layer of material; however, the density of that layer is linked to the deposition rate of the particles and therefore the electric field and the deposition voltage.[17,29] Insufficient deposition time will result in non-uniformity, pinholes, and small pores in the deposit, which will lead to lower power density.[9–12,14–17] This explains why the deposition voltage–deposition time interaction was significant in the power density model.

(3) ASR

A quadratic regression model was developed for ASR between the electrolyte and the two electrodes. After model reduction, the significant effects were firing temperature, voltage, the firing temperature–voltage interaction, and a quadratic voltage term, as shown in Table VII. The regression equation is given and regression coefficients with their corresponding *t* values are listed in Table VIII:

$$\begin{aligned}\text{ASR} = {} & 0.47437 + 2.65342 \times \text{firing temperature} \\ & + 0.33127 \times \text{voltage} \\ & + 0.28531 \times \text{firing temperature} \times \text{voltage} \\ & + 2.94295 \times \text{voltage}^2\end{aligned}$$

Figures 5(a)–(c) shows the ASR surface response and interaction plots. No single factor plots are shown because all factors

Table VII. Analysis of Variance (ANOVA) of Reduced Area-Specific Resistance Quadratic Model

Source	Sum of squares	Degrees of freedom	Mean square	*F*-value	*p*-value probability > *F*
Block	14.816	1	14.816		
Model	147.715	4	36.929	120.67	<0.0001
Firing temperature	119.550	1	119.550	390.64	<0.0001
Voltage	1.863	1	1.863	6.09	0.0223
Firing Temperature × voltage	1.302	1	1.302	4.26	0.0517
Voltage^2	24.999	1	24.999	81.69	<0.0001
Residual	6.427	21	0.306		
Lack of fit	4.201	10	0.420	2.08	0.1233
Pure error	2.226	11	0.202		
Cor total	168.958	26			

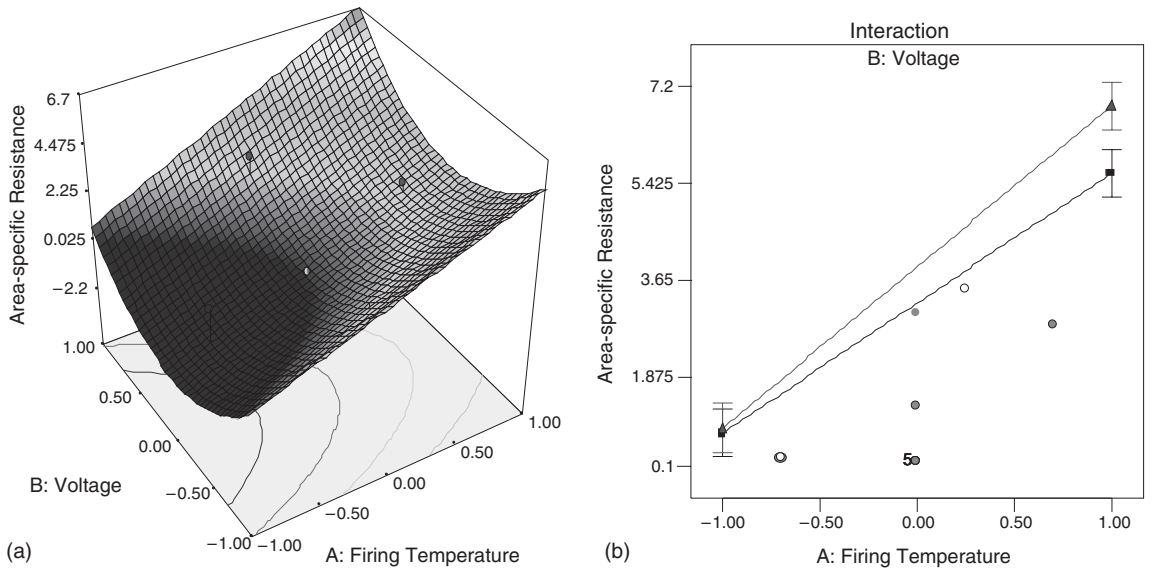

Fig. 5. (a) Surface response plot for area-specific resistance model, along with the (b) deposition voltage–deposition time interaction plot. Note that for the interaction plot, ▲ represents the high factor level and ■ represents the low factor level.

are also present in interactions. Although the R^2 values are high and the model contains a quadratic term, there is no evidence of "overfitting," as the model error ($S_{y.x} = 0.553$) is higher than the experimental error ($S_{\text{test}} = 0.449$). Although there are no apparent trends in the diagnostic plots, the Box–Cox plot did recommend a square root transform, which had a negligible effect on the model statistics and in the end was not used. Experimental run #27 was found to be close to the outlier threshold according to the externally studentized residual plot; however, its Cook's distance and leverage were comparable to all other samples. This point was not deleted when establishing the model. Model reduction resulted in only a small decrease in the amount of total variability explained by the model. In fact, the reduced model is able to explain a greater amount of variability (adjusted R^2 remained constant at 0.95) and is a better predictor of experimental data (predicted R^2 increased from 0.897 to 0.935) than the unreduced model.

Substrate firing temperature increases the ASR between the electrolyte and the electrodes, as seen in the regression equation and Fig. 5(a). The major contributor to increasing area-specific resistance with firing temperature is loss in substrate porosity. Porosity is believed to be fundamental to the deposition process on non-conducting substrates, as dense non-conducting substrates do not exhibit any deposit. Therefore, any decrease in porosity should hinder the deposition process and lead to increased area-specific resistance. Another possible contributor to ASR increase is the reduced curvature of the particle surface due to the higher firing temperature. It is conceivable that reducing the particle curvature could affect the deposition process if there is in fact a charge transfer step. A fundamental study to separate the contributions of porosity and degree of particle coarsening was not performed; however, it will be a necessary part of any future study to determine the deposition mechanism.

Table IX. Predicted Versus Experimental Values for the Model Validation Experiment

	Predicted values	Experimental values	Error (%)
Power density (mW/cm^2)	628	616	1.91
Area-specific resistance ($\Omega \cdot$ cm^2)	0.187	0.192	2.67
Deposition thickness (μm)	25.7	25.9	0.78

Voltage has the largest overall effect on ASR. The non-linear relationship shown in Fig. 5(a) indicates that the highest ASR values occur at the highest voltage levels. Deposit porosity and uniformity is directly linked to applied voltage, and area-specific resistance is highly dependent on surface area contact/coverage. Increasing the voltage should lead to a more porous deposit layer and higher ASR due to less contact area. The regression equation also includes a relatively weak firing temperature–voltage interaction. Therefore, to minimize ASR, the firing temperature should be low to ensure sufficient porosity and the voltage should also be relatively small in order to obtain a dense deposit of high contact area.

(4) Model Validation

After all the experiments and appropriate response models were completed, a final validation and optimization experiment was performed. The numerical optimization feature of Design Expert v.7 (Stat-Ease Inc.) allowed the preparation of an experiment based on a set of input criteria. The independent factors were all set to be in the range of the experimental matrix and the responses were set at desired levels: deposition thickness was set to be in the range of the experimental matrix, power density was set to be maximized, and ASR was set to be minimized. The solution with the highest level of desirability for achieving the optimum conditions was predicted to be experimental run #28, as listed in Table II. Table IX lists the predicted results based on the numerical solution and the actual experimental results for the validation experiment. There is a good correlation between the predicted and experimental results as seen with the low error, suggesting that the model can predict data accurately.

V. Conclusion

EDP of YSZ on porous non-conducting NiO–YSZ substrates was analyzed experimentally through an inscribed central composite statistical design. YSZ deposit thickness, power density, and ASR were influenced the greatest by the level of substrate firing temperature due to the resultant substrate porosity. Power density and ASR were also strongly influenced by the voltage quadratic term. Low levels of substrate firing temperature (1100°C), when combined with low levels of voltage (50 V) and time (1 min), lead to a 6 μm film with high power density (628 mW/cm^2) and low interfacial resistance (0.21 $\Omega \cdot$ cm^2). Substrate firing temperature and/or voltage increases generally

decreased deposit density and power density while increasing ASR. The time factor had its most significant influence on the deposit thickness and therefore also the power density, but was not found to affect ASR. A final experiment, generated by the model, validated the legitimacy of the model to predict experimental results.

Acknowledgment

This work was supported by the NASA URETI on UAPT program and the US Department of Energy SECA Core Technology Program (under Award Number DE-FC26-02NT41572). One of the authors (L. B.) is grateful to the Department of Science and Technology (DST), Goverment of India, for the BOYSCAST fellowship.

References

[1]N. Q. Minh and T. Takahashi, *Science and Technology of Ceramic Fuel Cells*. Elsevier Science BV, Amsterdam, 1995.

[2]S. C. Singhal, "Solid Oxide Fuel Cells for Stationary, Mobile and Military Applications," *Solid State Ionics*, **405–410**, 152–3 (2002).

[3]M. C. Williams, J. P. Strakey, and W. A. Surdoval, "The U.S. Department of Energy, Office of Fossil Energy Stationary Fuel Cell Program," *J. Power Sources*, **143**, 191–6 (2005).

[4]M. C. Williams and S. C. Singhal, "Mass-Produced Ceramic Fuel Cells for Low-Cost Power," *Fuel Cells Bull*., **24**, 8–11 (2000).

[5]F. Tietz, H.-P. Buchkremer, and D. Stover, "Components Manufacturing for Solid Oxide Fuel Cells," *Solid State Ionics*, **373–381**, 152–3 (2002).

[6]S. P. S. Badwal and K. Foger, "Solid Oxide Electrolyte Fuel Cell Review," *Ceram. Int*., **22**, 257–65 (1996).

[7]J. Will, A. Mitterdorger, C. Kleinlogel, D. Perednis, and L. J. Gaukler, "Fabrication of Thin Electrolytes for Second-Generation Solid Oxide Fuel Cells," *Solid State Ionics*, **131**, 79–96 (2000).

[8]H. Ohuri, T. Matsushima, and T. Hirai, "Performance of a Solid Oxide Fuel Cell Fabricated by Co-Firing," *J. Power Sources*, **71**, 185–9 (1998).

[9]T. Ishihara, K. Sato, Y. Mizuhara, and Y. Takita, "Preparation of Yittria-Stabilized Zirconia Films for Solid Oxide Fuel Cells by Electrophoretic Deposition Method," *Chem. Lett*., 943–6 (1992).

[10]T. Ishihara, K. Sato, and Y. Takita, "Electrophoretic Deposition of Y_2O_3-Stabilized ZrO_2 Electrolyte Films in Solid Oxide Fuel Cells," *J. Am. Ceram. Soc*., **79** [4] 913–9 (1996).

[11]T. Ishihara, K. Shimose, T. Kudo, H. Nishiguchi, T. Akbay, and Y. Takita, "Preparation of Yittria-Stabilized Zirconia Thin Films on Strontium-Doped $LaMnO_3$ Cathode Substrates Via Electrophoretic Deposition for Solid Oxide Fuel Cells," *J. Am. Ceram. Soc*., **83** [8] 1921–7 (2000).

[12]F. Chen and M. Liu, "Preparation of Yittria-Stabilized Zirconia (YSZ) Films on $La_{0.8}Sr_{0.2}MnO_3$ (LSM) and LSM-YSZ Substrates Using an Electrophoretic Deposition (EPD) Process," *J. Eur. Ceram. Soc*., **21**, 127–34 (2001).

[13]I. Zhitomirsky and A. Petric, "Electrophoretic Deposition of Ceramic Materials for Fuel Cell Applications," *J. Eur. Ceram. Soc*., **20**, 2055–61 (2000).

[14]J. Will, M. K. M. Hruschka, L. Gubler, and L. J. Gauckler, "Electrophoretic Deposition of Zirconia on Porous Anodic Substrates," *J. Am. Ceram. Soc*., **84** [2] 328–32 (2001).

[15]K. Kobayashi, I. Takahashi, M. Shiono, and M. Dokiya, "Supported $Zr(Sc)O_2$ SOFCs for Reduced Temperature Prepared by Electrophoretic Deposition," *Solid State Ionics*, **591–596**, 152–3 (2002).

[16]K. Yamaji, H. Kishimoto, Y. Xiong, T. Horita, N. Sakai, and H. Yokokawa, "Performance of Anode-Supported SOFCs Fabricated with EPD Techniques," *Solid State Ionics*, **175**, 165–9 (2004).

[17]M. Matsuda, T. Hosomi, K. Murata, T. Fukui, and M. Miyake, "Direct EPD of YSZ Electrolyte Film onto Porous NiO-YSZ Composite Substrate for Reduced-Temperature Operating Anode-Supported SOFC," *Electrochem. Solid State Lett*., **8** [1] A8–11 (2005).

[18]D. C. Montgomery, *Design and Analysis of Experiments*, 5th edition, John Wiley & Sons, New York, 2001.

[19]R. Verseput, "Digging into DOE," *Quality Digest* [Electronic version] **21** [6] (2001).

[20]L. Besra, C. Compson, and M. Liu, *J. Am. Ceram. Soc*, accepted.

[21]R. H. Myers and D. C. Montgomery, *Response Surface Methodology*. John Wiley & Sons, New York, 1995.

[22]H. C. Hamaker and E. J. W. Verway, "The Role of the Forces Between the Particles in Electrode Position and other Phenomenon," *Trans. Faraday Soc*., **36**, 180–5 (1940).

[23]W. F. Pickard, "Remarks on the Theory of Electrophoretic Deposition," *J. Electrochem. Soc*., **115**, 105C–8C (1968).

[24]D. R. Brown and F. W. Salt, "The Mechanism of Electrophoretic Deposition," *J. Appl. Chem*., **15**, 40–8 (1965).

[25]J. Mizuguchi, K. Sumi, and T. Muchi, "A Highly Stable Non-Aqueous Suspension for Electrophoretic Deposition of Powdered Substances," *J. Electrochem. Soc*., **130**, 1819–25 (1983).

[26]P. Sarkar and P. S. Nicholson, "Electrophoretic Deposition (EPD): Mechanisms, Kinetics and Applications to Ceramics," *J. Am. Ceram. Soc*., **79** [8] 1987–2002 (1996).

[27]G. Anne, K. Vanmeensel, J. Vleugels, and O. Van der Biest, "Influence of the Suspension Composition on the Electric Field and Deposition Rate During Electrophoretic Deposition," *Colloids Surf. A*, **245**, 35–9 (2004).

[28]H. C. Hamaker, "Formation of a Deposit by Electrophoresis," *Trans. Faraday Soc*., **36**, 279–87 (1940).

[29]I. Zhitomirsky and A. Petric, "Electrophoretic Deposition of Ceramic Materials for Fuel Cell Applications," *J. Eur. Ceram. Soc*., **20**, 2055–61 (2000).

[30]F. Bouyer and A. Foissy, "Electrophoretic Deposition of Silicon Carbide," *J. Am. Ceram. Soc*., **82** [8] 2001–10 (1999). □